Noise Dissipation Mechanisms in a Multi-Cavity Acoustic Liner Grazed by Turbulent Flow and Acoustic Waves

Noise dissipation mechanisms in a multi-cavity acoustic liner grazed by turbulent flow and acoustic waves

Francesco Scarano *, Angelo Paduano† and Francesco Avallone‡
Politecnico di Torino, Corso Duca degli Abruzzi 24, 10122, Torino, Italy

High-fidelity lattice-Boltzmann very-large-eddy simulations are used to analyse the acoustic energy dissipation mechanisms over a 22-cavities single-degree-of-freedom liner with chamfered orifices, subjected to grazing turbulent flow and acoustic plane wave at 145 dB. The analysis extends previous single-cavity investigations by accounting for the streamwise development of the grazing flow and the associated decay of the sound pressure level (SPL) along the liner. The results show that, in the absence of grazing flow, acoustic dissipation is dominated by vortex shedding in the upstream cavities, where the SPL is sufficiently high, and by viscous effects downstream as the SPL decreases. The dissipation is concentrated in the first portion of the liner, where nonlinear effects are strongest. When grazing flow is introduced, the flow topology inside the orifice is significantly modified. A quasi-steady vortex forms in the upstream portion of the orifice, redistributing the acoustic-induced velocity and concentrating viscous dissipation on the downstream lip during the inflow phase. At the same time, vortex shedding becomes phase dependent, contributing to dissipation during inflow and to acoustic energy generation during outflow, resulting in a net negative contribution. The combined effect leads to a redistribution of dissipation along the liner, with an approximately uniform streamwise behaviour arising from the balance between enhanced viscous dissipation and vortex-shedding generation. These results explain the reduced liner performance in the presence of grazing flow and highlight the importance of accounting for grazing flow in liner analysis and design.

I. Introduction

Acoustic liners are widely employed in the inlet and bypass ducts of aircraft engines as passive noise control devices to mitigate fan noise emissions [1, 2]. The developement of ultra-high bypass ratio engines, characterized by larger fan diameters and reduced rotational speeds, has heightened the relative importance of fan noise to the overall engine acoustic signature. This noise component consists of discrete tones at the Blade Passing Frequency (BPF) and broadband contributions arising from turbulence impingement in the fan–stator region [3–5]. The tonal component is typically dominant and confined within narrow frequency bands, which makes it particularly suitable for attenuation using acoustic liners.

The simplest liner configuration is the single-degree-of-freedom (SDOF) liner, consisting of a perforated facesheet backed by a cavity. In the absence of grazing flow, the liner behaves as a Helmholtz resonator whose acoustic response depends on its geometric parameters and can be tuned to target specific frequencies, such as the BPF [6]. At low sound pressure levels (SPL), acoustic dissipation is dominated by viscous effects at the orifice walls, as demonstrated by the numerical analysis of Tam and Kurbatskii [7] in the absence of grazing flow. As the SPL increases, the regime becomes nonlinear and is characterized by vortex shedding at the orifice neck [8, 9], whereby acoustic energy is converted into turbulent kinetic energy and eventually dissipated as heat.

High-fidelity simulations by Scarano et al. [10] have provided a detailed characterization of these dissipation mechanisms in a single-cavity configuration both in presence and in absence of grazing flow. In the absence of grazing flow, viscous and vortex-shedding contributions act over both inflow and outflow phases, with vortex shedding dominating at high SPL. When a grazing flow is introduced, the flow topology inside the orifice is significantly altered: the shear layer at the orifice mouth generates a quasi-steady vortex that confines the acoustic-induced motion to the downstream portion of the orifice. This modification leads to an increase of viscous dissipation at low SPL and to a phase-dependent vortex-shedding contribution, which dissipates acoustic energy during inflow and can generate acoustic energy during outflow. As a result, the net acoustic dissipation is reduced in the presence of grazing flow. However,

*Research fellow, Department of Mechanical and Aerospace Engineering, francesco.scarano@polito.it.
†PhD student, Department of Mechanical and Aerospace Engineering, angelo.paduano@polito.it.
‡Full Professor, Department of Mechanical and Aerospace Engineering, francesco.avallone@polito.it, AIAA member.

these results were obtained for an isolated cavity and therefore do not account for the streamwise development of the grazing flow and its cumulative interaction with multiple cavities.

While most studies have focused on isolated cavities or liners in simplified conditions, real engine liners consist of multiple interacting cells exposed to a developing turbulent grazing flow. Both experimental and numerical investigations have shown that geometric features such as orifice diameter, thickness, and distribution affect liner impedance and acoustic absorption [11–14]. A recent study by Paduano et al. [15] have shown that a multiple cavity acoustic liner can significantly modify the grazing flow through the coupling between acoustic forcing and turbulent fluctuations. The presence of the orifices displaces the flow away from the facesheet, leading to a streamwise growth of the boundary layer displacement thickness and the formation of localised distortions downstream of each cavity. As the flow develops, the shear layer at the orifice mouth weakens in the downstream direction, modifying the effective interaction between the acoustic field and the liner. These results demonstrate that the near-wall flow topology varies along the liner and that the flow field experienced by the acoustic waves is inherently non-uniform, suggesting the importance to extend the dissipation analysis to a full liner configuration.

The present work extends the analysis of Scarano et al. [10] from a single-cavity configuration to a full SDOF liner, explicitly accounting for the streamwise development of the turbulent grazing flow. The objective is to investigate how the combined effects of flow evolution along the liner and the progressive decay of the SPL influence the local flow–acoustic interaction and the overall noise absorption capability of the liner. A numerical dataset consisting of a liner with multiple cavities subjected to grazing acoustic waves is employed. The results are compared against the same configuration in the absence of grazing flow. The acoustic energy dissipation mechanisms are quantified consistently with Scarano et al. [10]: viscous losses at the orifice walls are evaluated following Tam and Kurbatskii [7], while the acoustic-to-vortical energy conversion associated with vortex shedding is computed using Howe's energy corollary [8]. By analysing the streamwise evolution of these contributions and their relation to the local flow topology and SPL variation, this study provides new insight into how grazing flow development modifies liner performance at both local and global scales.

II. Numerical setup and database description

The simulations analyzed in this work are part of a numerical database developed for two companion papers presented at this conference. While the paper by Paduano et al. [16] provides a detailed description of the numerical setup, solver formulation, and impedance evaluation, the present study focuses on the analysis of the dissipation mechanisms. For completeness, the main features of the computational model are summarized below.

The computational domain, shown in Figure 1, reproduces the main characteristics of the Federal University of Santa Catarina (UFSC) Liner Test Rig. A turbulent grazing flow develops over the liner mounted on the upper wall of a rectangular duct, with a uniform inlet velocity equal to a Mach number of 0.3 ($U_0 = 110$ m/s) and a pressure outlet boundary condition.

In the the full dataset reported by Paduano et al. [16], two liner configurations are investigated, differing only in the orifice-edge geometry: a reference sharp-edged design and a chamfered-edge variant (Figure 1c, d). All other geometric parameters are identical, including cavity width ($l = 12.46$ mm), depth ($\lambda = 38.10$ mm), orifice diameter ($d = 1.00$ mm), facesheet thickness ($\tau = 0.56$ mm), and partition wall thickness ($w_p = 2.53$ mm). Each cavity contains eight orifices, and a total of 22 cavities are modeled along the streamwise direction. Lateral periodic boundary conditions are applied, consistent with previous numerical studies that demonstrated negligible influence on the acoustic response [17].

The simulations were performed using the commercial software 3DS Simulia PowerFLOW version 6 using a high-fidelity lattice Boltzmann/very-large-eddy simulation (LB/VLES) framework. The mesh employs a variable resolution (VR) approach, with the finest grid level (corresponding to approximately 40 cells) across each orifice diameter with a total of $O(10^8)$ computational cells. This mesh density was selected based on prior sensitivity studies, which demonstrated that further refinement yields negligible impact on the simulated results [15]. A two-step simulation strategy was adopted. First, a statistically converged turbulent flow field was obtained under grazing flow conditions. Then, a plane acoustic wave of prescribed frequency and amplitude was superimposed using the *OptydB* toolkit [18]. This method explicitly resolves the nonlinear interaction between the turbulent grazing flow and the imposed acoustic field, allowing accurate characterization of dissipation mechanisms.

A total of forty simulations were carried out, spanning different acoustic frequencies, sound pressure levels and acoustic propagation directions with respect to the grazing flow. In the present work, we focus on a subset of these cases to investigate the streamwise evolution of the acoustic energy dissipation along the chamfered liner in presence and in absence of grazing flow at 145 dB at a source frequency of 1400 Hz. The analysis is performed on a two-dimensional

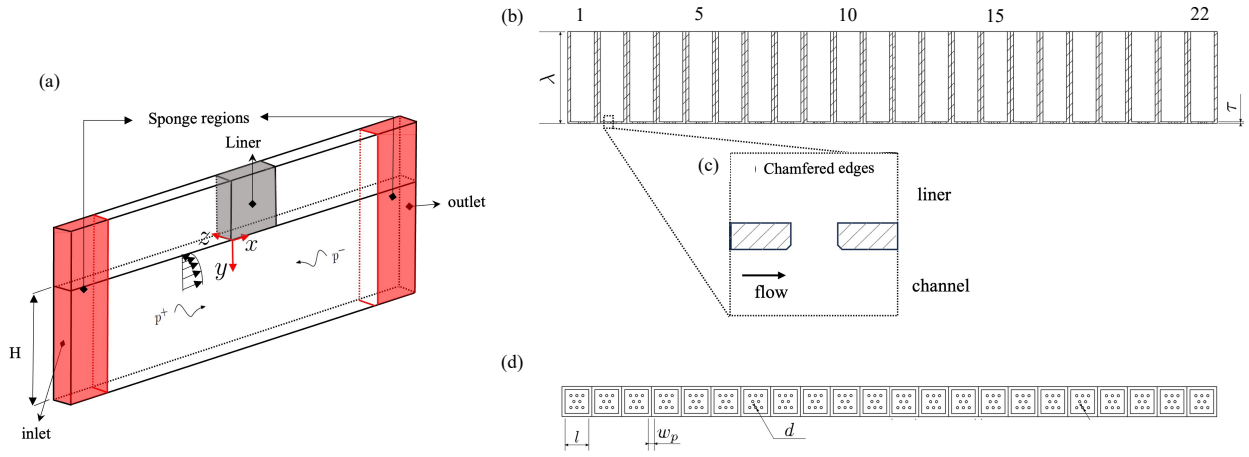

Fig. 1 Sketch of the numerical setup (a) 3D geometry, (b) 2D cross-plane of the acoustic liner, (c) sketch of the orifice shape, (d) facesheet detail of the liners.

streamwise slice extracted from the simulations over the middle of the liner, covering two consecutive orifices per cavity and the adjacent portions of the cavity and the upper and lower channel. As shown by Scarano et al. [10], where both two- and three-dimensional analyses were conducted, the two-dimensional representation provides a reliable estimate of the dissipation mechanisms within the orifice.

III. Data reduction methodology

A. Nomenclature for velocity components

The instantaneous velocity field is denoted by $\boldsymbol{u}'$ and decomposed as

$$\boldsymbol{u}' = \boldsymbol{U} + \boldsymbol{u}, \tag{1}$$

where $\boldsymbol{U}$ is the mean velocity and $\boldsymbol{u}$ the fluctuating component. The velocity vector is $\boldsymbol{u}' = (u', v', w')$ in the (x, y, z) directions, with U, V, W the mean components and u, v, w the fluctuations. In the presence of acoustic forcing, $\boldsymbol{u}$ includes both turbulent fluctuations and the acoustic-induced velocity $\boldsymbol{u}_{\mathrm{ac}}$, associated with the periodic forcing [19].

B. Acoustic dissipation by viscous effects

The viscous dissipation is evaluated from the instantaneous velocity field following Tam and Kurbatskii [7]. The local volumetric dissipation density is

$$\Phi(\boldsymbol{x}, t) = \sigma_{ij} \frac{\partial u_i'}{\partial x_j}, \tag{2}$$

with viscous stress tensor

$$\sigma_{ij} = \mu \left(\frac{\partial u_i'}{\partial x_j} + \frac{\partial u_j'}{\partial x_i} \right), \tag{3}$$

where μ is the dynamic viscosity and $\boldsymbol{x} = (x, y, z)$. The quantity Φ represents the irreversible conversion of mechanical energy into heat.

To isolate acoustically induced viscous losses, the integration is restricted to a near-wall region of the orifice (up to ≈ 30 wall units, $\Delta x/d < 0.09$), excluding background dissipation from the grazing turbulent boundary layer. The viscous dissipation rate in a control volume V is

$$D(t) = \iiint_V \Phi(\boldsymbol{x}, t)\, \mathrm{d}V. \tag{4}$$

This choice captures near-wall gradients and viscous stresses within the orifice, consistent with resonant liner formulations [7]. Dissipation associated with turbulent cascade in the bulk flow is not included here and is instead accounted for through the vortex-shedding contribution.

The phase-dependent dissipation is obtained as $D(\phi)$, and the net viscous energy per period T is

$$E_{\text{viscous}} = \frac{1}{T}\int_0^T D(\phi)\,\mathrm{d}\phi = \iiint_V e_{\text{viscous}}\,dV. \tag{5}$$

where e_{viscous} [W/m^3] is the is the time averaged volumetric dissipation density within the domain of the orifice.

All quantities are normalized in wall units using $u_\tau = \sqrt{\tau_w/\rho}$ and $\delta_\nu = \nu/u_\tau$. The normalized forms are

$$\Phi^+ = \frac{\Phi}{\rho u_\tau^4 \nu}, \qquad e^+_{\text{viscous}} = \frac{e_{\text{viscous}}}{\rho u_\tau^4/\nu}, \qquad D^+ = \frac{D}{\rho \nu^2 u_\tau}. \tag{6}$$

C. Acoustic energy conversion into vortex shedding

The conversion of acoustic energy into vortical motion is quantified using Howe's corollary [8, 20, 21]. The local power density is

$$\Pi_g(\boldsymbol{x}, t) = \rho\,(\boldsymbol{\omega} \times \boldsymbol{u}') \cdot \boldsymbol{u}_{\text{ac}}, \tag{7}$$

where $\boldsymbol{\omega}$ is the vorticity. The total conversion rate over a control volume V is

$$\Pi(t) = \iiint_V \Pi_g(\boldsymbol{x}, t)\,\mathrm{d}V. \tag{8}$$

The control volume includes the orifice, cavity, shear layer, and interacting portion of the grazing boundary layer to capture the dominant acoustic–vortical interactions.

The phase-averaged quantity is $\Pi^+(\phi)$, and the net energy transfer over one period is

$$E_{\text{shedding}} = \frac{1}{T}\int_0^T \Pi(\phi)\,\mathrm{d}\phi = \iiint_V e_{\text{shedding}}\,dV. \tag{9}$$

where e_{shedding} [W/m^3] is the is the time averaged volumetric dissipation density within the domain of the orifice.

The normalized quantities are

$$\Pi_g^+ = \frac{\Pi_g}{\rho u_\tau^4/\nu}, \qquad e^+_{\text{shedding}} = \frac{e_{\text{shedding}}}{\rho u_\tau^4/\nu} \qquad \Pi^+ = \frac{\Pi}{\rho \nu^2 u_\tau}. \tag{10}$$

Positive values indicate absorption of acoustic energy by the vortical field, while negative values indicate generation.

D. Acoustic-induced velocity estimation

The acoustic-induced velocity is extracted using Spectral Proper Orthogonal Decomposition (SPOD) [22], following Scarano et al. [19]. SPOD is applied to time-resolved velocity fluctuations over multiple acoustic cycles and provides frequency-dependent modes ranked by energy. The acoustic velocity is reconstructed from the leading mode at the forcing frequency via a narrow-band selection, isolating the coherent, phase-locked component.

For flows with a single dominant forcing and no additional tonal sources, this approach is equivalent to Coherent Component Decomposition (CCD) [23]. Compared to classical phase-averaging used in liner studies (e.g. [24, 25]), SPOD provides a more robust separation between coherent acoustic motion and broadband turbulence in the presence of grazing flow [19].

The term "acoustic-induced velocity" denotes the component coherent with the forcing frequency, not a strictly irrotational field. Methods based on Helmholtz decomposition or acoustic equations require full three-dimensional information and assumptions not satisfied in the present configuration. The SPOD-based approach therefore provides a consistent and practical estimate of the velocity field relevant to the acoustic energy-transfer analysis.

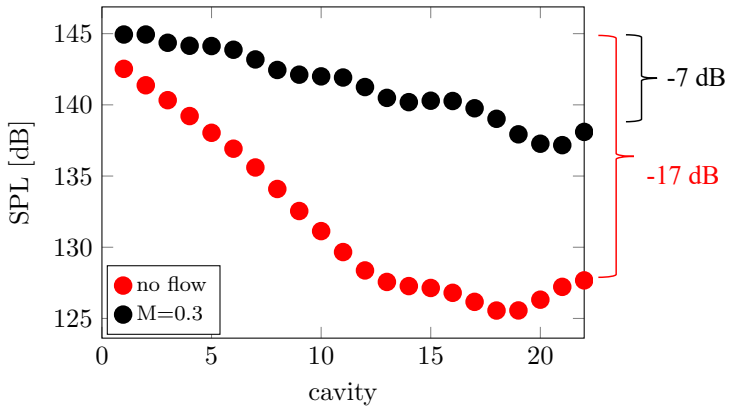

Fig. 2 Comparison of SPL decays over the liner with and without grazing flow, source frequency 1400 Hz, incident SPL = 145 dB.

IV. Results

A. SPL decay

Before analysing the dissipation mechanisms, the streamwise distribution of the overall SPL is presented in figure 2. The SPL is evaluated in the upstream portion of each cavity within in the location farthest from the wall of the analyzed domain, so, in presence of grazing flow, it takes into account also the additional pressure fluctuation provided by the turbulent field.

In the absence of grazing flow, the SPL decreases monotonically along the liner up to cavity 19, indicating progressive absorption of the incident acoustic energy. As a result, the downstream cavities are exposed to a reduced acoustic amplitude. A moderate increase in SPL is observed in the last cavities (20-22), which is attributed to impedance sudden variation (perforated-smooth surface) and the associated reflection of acoustic waves.

When a turbulent grazing flow is introduced, the SPL distribution changes substantially. The first cavity exhibits a slightly higher SPL compared to the no-flow condition, consistent with grazing flow acting as an additional broadband noise source [26]. Similarly to the case in absence of grazing flow the change in impedance boundary condition leads to reflected acoustic waves which increase the SPL over the last cavities. More importantly, the decay of SPL along the liner is significantly reduced, indicating a degradation of the liner acoustic performance. The total SPL decay decreases from approximately -17 dB in the absence of flow to -7 dB with grazing flow. This highlights a strong degradation of the liner performance.

This reduced performance arises from two coupled effects. The interaction between the grazing flow and the acoustic waves modifies the local flow–acoustic coupling and dissipation mechanisms, this in turn modifies the liner impedance, altering the balance between transmitted and reflected acoustic energy. The first aspect is investigated in the following sections through a detailed analysis of the underlying dissipation mechanisms.

B. Acoustic-induced velocity

To highlight the modification of the flow topology inside the orifice at different streamwise locations (i.e. for different cavity numbers), the acoustic-induced velocity in wall units is presented in figures 3 (no flow) and 4 (with grazing flow) during the inflow ($\phi = \pi/2$) and outflow ($\phi = 3\pi/2$) phases. Contours for cavities 1, 10, and 22 are shown in subfigures (a-c), while subfigure (d) reports the corresponding velocity profiles for cavities 1, 5, 10, 15, and 22 taken at the centreline of the orifice ($y/\tau = 0.5$). Subfigure (e) shows the profiles between the first and second orifice for a selected cavity.

In the absence of grazing flow, the acoustic-induced velocity is relatively evenly distributed within the orifice, with a maximum located in the upstream half. This behaviour is attributed to the grazing acoustic waves and can be further enhanced by the chamfered geometry, which promotes flow penetration into the orifice, and differs from sharp-edged configurations [10, 15, 19]. Similar results were reported by Avallone et al. [27] in absence of grazing flow for normal impedance tube simulations. Both contour plots and velocity profiles show a progressive decrease in acoustic-induced velocity in the streamwise direction, consistent with the decay of SPL along the liner. A similar reduction is observed

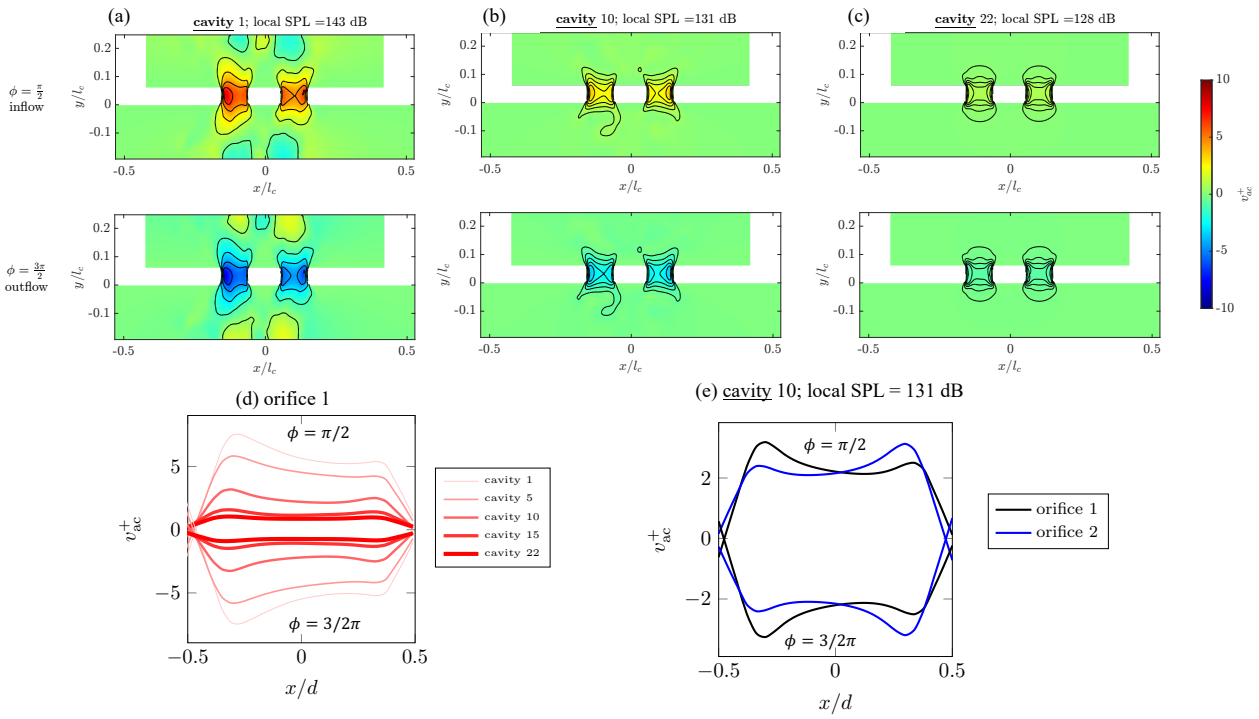

Fig. 3 Contour of the wall-normal acoustic induced velocity v^+_{ac} in inflow and outflow phases at $M = 0$, forcing frequency equal to 1400 Hz,incident SPL = 145 dB ϕ, (a) cavity 1, (b) cavity 10, (c) cavity 22; v^+_{ac} profiles at various phases taken at the centreline of the orifice (d) first orifice, effect of changing the cavity (e) cavity 10, comparison between orifice 1 and 2.

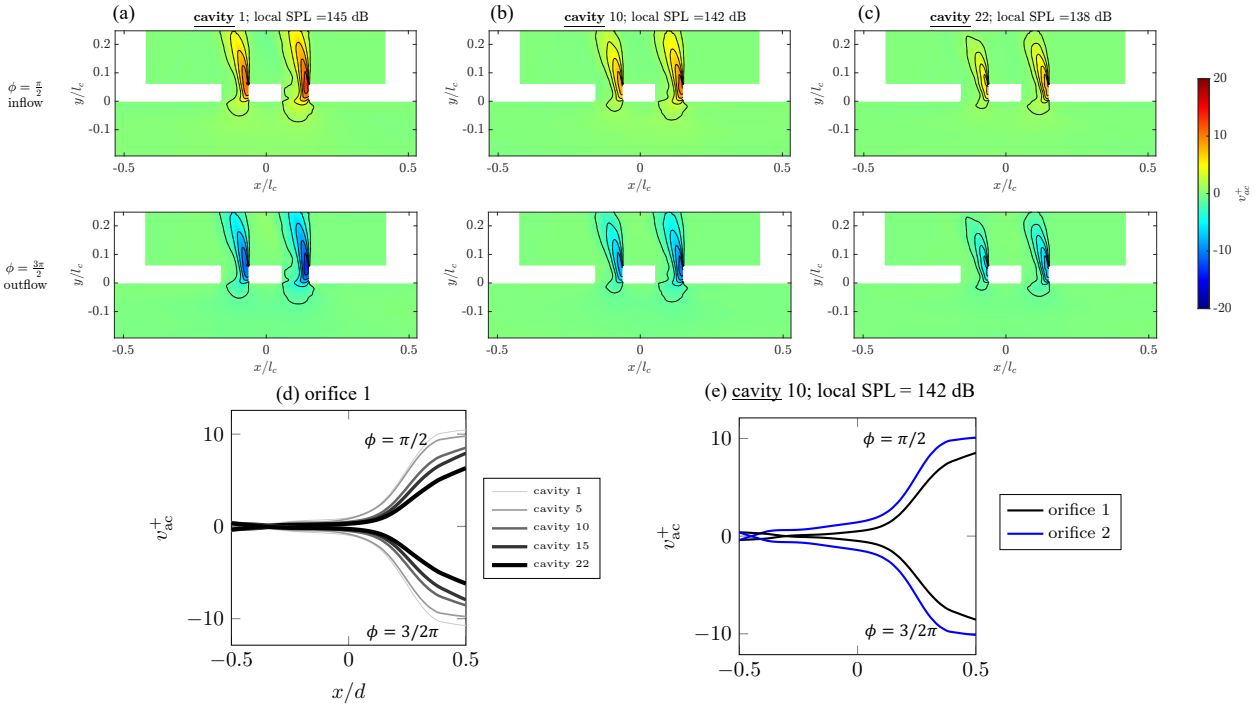

Fig. 4 Contour of the wall-normal acoustic induced velocity v^+_{ac} in inflow and outflow phases at $M = 0.3$, forcing frequency equal to 1400 Hz,incident SPL = 145 dB ϕ, (a) cavity 1, (b) cavity 10, (c) cavity 22; v^+_{ac} profiles at various phases taken at the centreline of the orifice (d) first orifice, effect of changing the cavity (e) cavity 10, comparison between orifice 1 and 2.

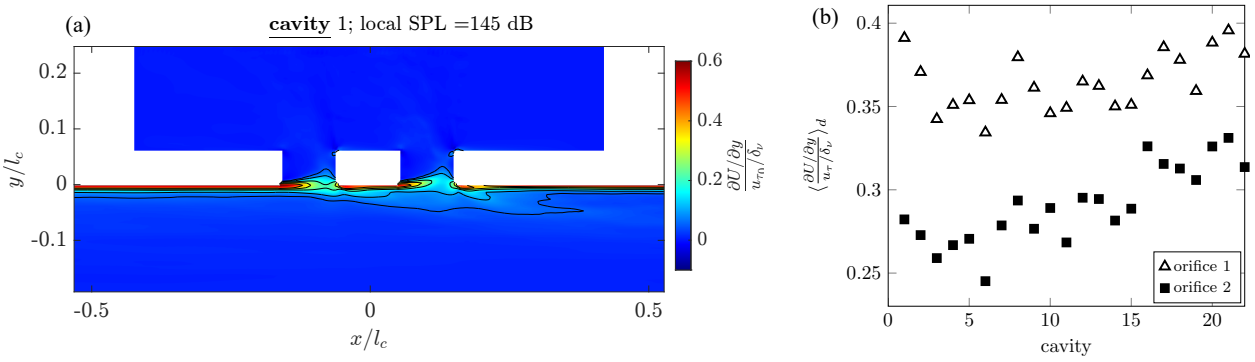

Fig. 5 Normalized shear layer over the cavity, (a) contour on the first cavity, (b) averaged normalized shear over the diameter for the first and second orifice as function of the cavity number.

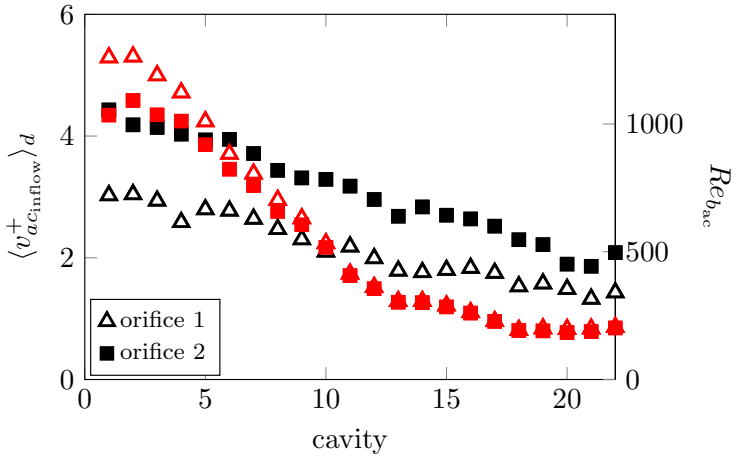

Fig. 6 Averaged acoustic-induced velocity in wall units in the inflow phase as function of the cavity number, on the right hand side the acoustic-induced bulk Reynolds number inside the orifice is reported.

between the first and second orifice for upstream cavities, while this effect becomes less pronounced further downstream where the SPL is already reduced.

This trend is better shown in figure 6, which shows the decrease of v^+_{ac}, averaged across the orifice, along the liner. The corresponding bulk Reynolds number based on the acoustic-induced velocity, computed during the inflow phase and averaged over the orifice diameter, also decreases rapidly in the streamwise direction, reaching values $Re^{ac}_b < 500$ downstream of the fifth cavity. This indicates that nonlinear effects associated with high SPL are primarily confined to the first portion of the liner.

When a turbulent grazing flow is introduced, the flow topology of the acoustic-induced velocity changes markedly, in agreement with Zhang and Bodony [28] and Paduano et al. [15]. The acoustic-induced velocity becomes concentrated in the downstream half of the orifice, exhibiting a jet-like structure during both inflow and outflow phases, while the upstream portion is occupied by a quasi-steady vortex associated with a vena contracta effect. This reduces the effective porosity of the orifice and increases flow blockage.

As shown in figure 4, the magnitude of v^+_{ac} still decreases in the streamwise direction, but less markedly than in the no-flow case, reflecting the reduced SPL decay. Interestingly, the trend between the first and second orifice is reversed: the acoustic-induced velocity in the second orifice is larger than in the first one (figure 4e). This is attributed to the combined effect of a weaker SPL decay and the modification of the shear layer by the upstream orifice. The jetting motion during the outflow phase displaces fluid away from the wall, increasing the displacement thickness and weakening the shear layer over the downstream orifice [15].

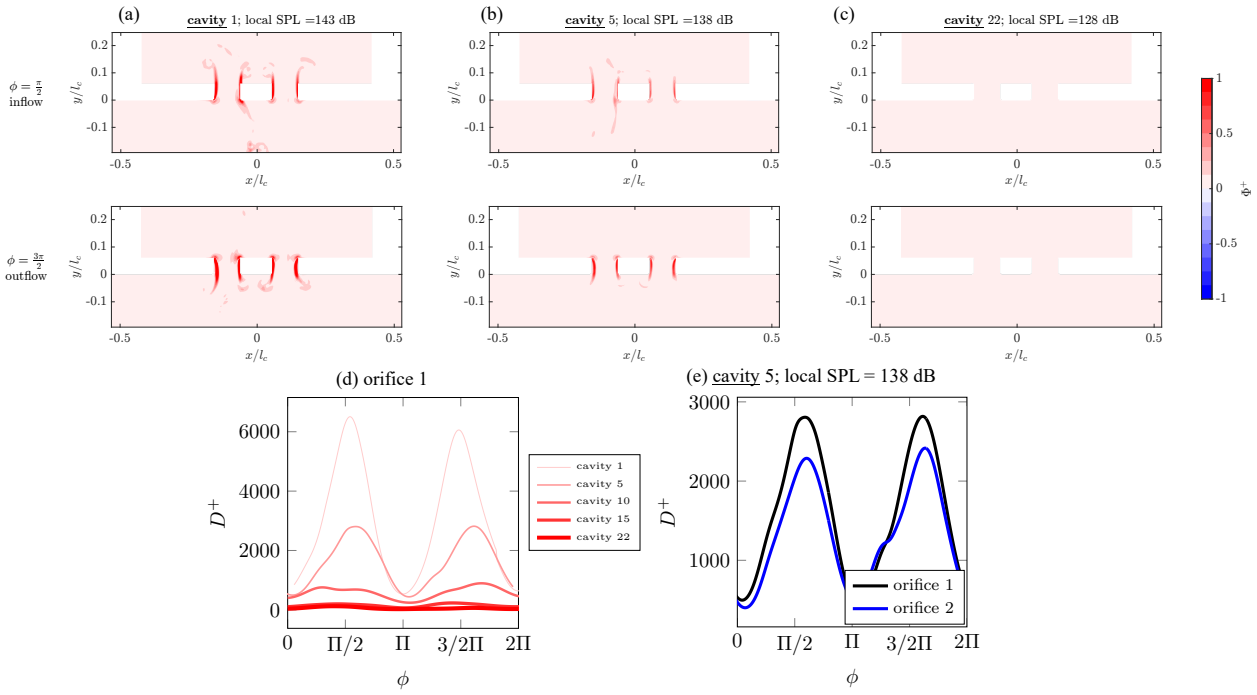

Fig. 7 Contour of the viscous dissipation density Φ^+ in inflow and outflow phases at $M = 0.$, forcing frequency equal to 1400 Hz,incident SPL = 145 dB; (a) cavity 1, (b) cavity 10, (c) cavity 22; viscous dissipation rate D^+ as a function of the phase, ϕ, (d) first orifice, effect of changing the cavity (e) cavity 10, comparison between orifice 1 and 2.

This effect is illustrated in figure 5(a), which shows contours of the normalized mean shear

$$\frac{\partial U/\partial y}{u_\tau/\delta_\nu}. \tag{11}$$

Only the grazing-flow case is reported, as the mean shear is relevant only in the presence of a mean flow. The second orifice clearly exhibits a weaker shear layer compared to the first one. This trend is confirmed in figure 5(b), where the shear averaged across the orifice diameter shows a systematic reduction for the second orifice.

The streamwise evolution of the shear indicates a rapid decrease of the shear over the first cavities, followed by a more gradual increase in the second half of the liner. This is result of the combined effects of boundary-layer development and SPL decay. As a consequence, although the acoustic-induced velocity decreases along the liner, the reduction is less pronounced than in the no-flow case. In particular, for the second orifice the bulk Reynolds number remains above $Re_b^{ac} \approx 500$ along the entire liner, indicating that nonlinear effects persist downstream and are sustained by the interaction of the acoustic waves with the grazing flow.

C. Acoustic dissipation by viscous effects at the mouth of the orifice

Figures 7 and 8 show the contours of the viscous dissipation density in wall units for the cases without and with grazing flow, respectively. Subfigures (a-c) report the contours during the inflow and outflow phases for cavities 1, 10, and 22 .

In the absence of grazing flow, symmetric boundary layers develop along the upstream and downstream edges of the orifice. As a result, viscous dissipation during the inflow and outflow phases is comparable, with a slight predominance during the outflow phase. This asymmetry is attributed to the sharp edge encountered during outflow, which promotes the formation of a thicker shear layer and enhances local dissipation. The dissipation decreases in the streamwise direction due to the decay of SPL and the corresponding reduction of v_{ac}^+. This trend is illustrated in subfigure (d), which reports the integrated dissipation for cavities 1, 5, 10, 15, and 22. Two lobes are observed, associated with inflow and outflow, whose magnitude progressively decreases downstream. Similarly to the behaviour of v_{ac}^+, the second

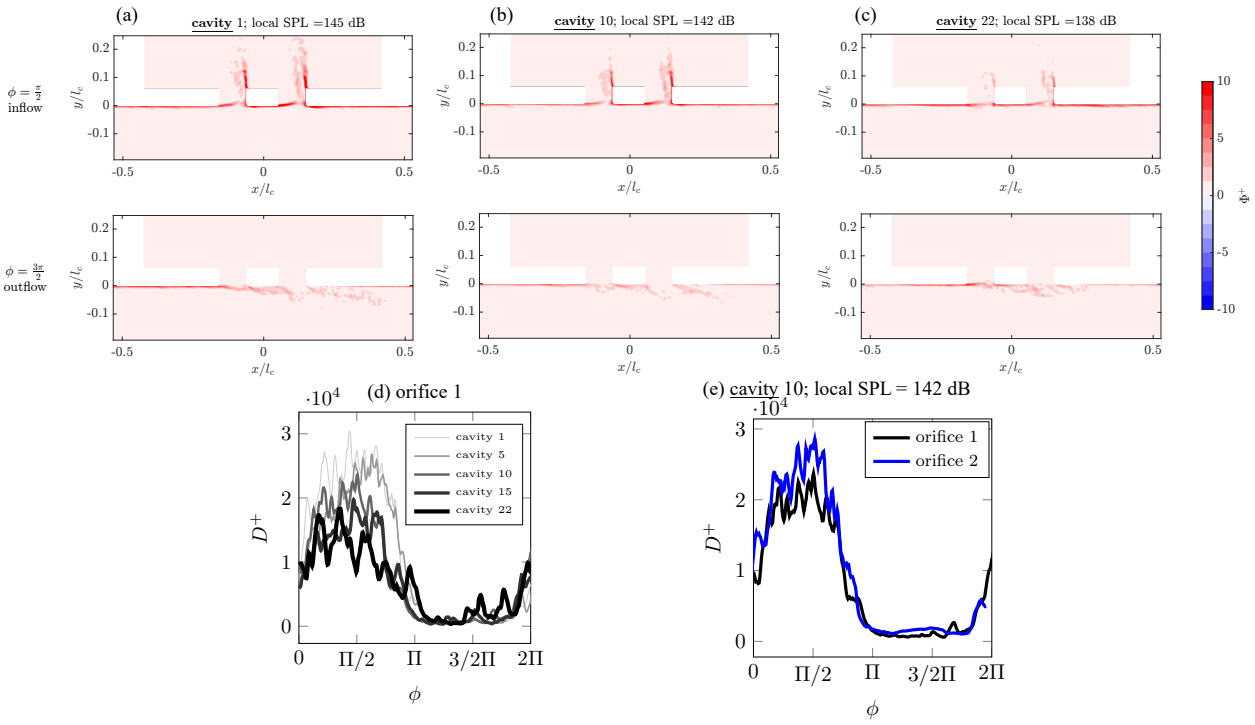

Fig. 8 Contour of the viscous dissipation density Φ^+ in inflow and outflow phases at $M = 0.3$, forcing frequency equal to 1400 Hz,incident SPL = 145 dB; (a) cavity 1, (b) cavity 10, (c) cavity 22; viscous dissipation rate D^+ as a function of the phase, ϕ, (d) first orifice, effect of changing the cavity (e) cavity 10, comparison between orifice 1 and 2.

orifice within a cavity exhibits lower viscous dissipation than the first one due to the local SPL reduction.

This symmetry is broken when grazing flow is introduced (figure 8). The upstream edge of the orifice exhibits a marked reduction in Φ^+ due to the formation of a vena contracta and the presence of a quasi-steady vortex occupying the upstream half of the orifice. Conversely, the downstream wall experiences stronger shear as the flow is deflected towards the downstream lip. As a result, viscous dissipation becomes concentrated along the downstream edge and predominantly during the inflow phase.

Figure 8(d) reports the phase-dependent viscous dissipation rate integrated along the orifice walls for selected cavities (1, 5, 10, 15, and 22). In the presence of grazing flow, the inflow-phase dissipation is significantly amplified with respect to the no-flow case due to the impingement of the acoustic-induced flow on the downstream edge. High-frequency fluctuations indicate intermittent penetration of turbulent structures into the orifice. In contrast, the outflow-phase dissipation becomes negligible, reflecting the partial blockage induced by the overlying shear layer. Consequently, the dissipation pattern becomes strongly asymmetric and governed by the interaction between acoustic forcing and the grazing turbulent flow. Consistently with the behaviour of the acoustic-induced velocity, the viscous dissipation in the second orifice is higher than in the first one, due to the locally increased v^+_{ac} resulting from the weakened shear layer.

D. Acoustic dissipation by vortex shedding

Figures 9 and 10(a–c) present the instantaneous acoustic power density Π^+_g associated with the exchange of energy between the acoustic field and vortical motions, in the absence and presence of grazing flow, respectively. Positive values of Π^+_g (red) indicate acoustic energy dissipated through vortex shedding, whereas negative values (blue) correspond to acoustic energy generation.

In the absence of grazing flow, two well-defined regions of positive Π^+_g appear near the orifice mouth during both inflow and outflow phases. These regions correspond to region of conversion of acoustic energy into the formation and roll-up of vortices driven by the acoustic-induced velocity. Cavity 5 is reported, as further downstream the shedding contribution becomes negligible due to the reduced SPL and low Re^{ac}_b. Similarly to viscous dissipation, the outflow phase exhibits a slightly stronger contribution due to the sharp edge encountered by the flow, which promotes vortex formation. This behaviour is confirmed in subfigure (d), where the cycle-resolved shedding rates Π^+ are reported for selected cavities. Two distinct lobes are observed, associated with inflow and outflow phases. The magnitude of the shedding contribution decreases rapidly in the streamwise direction and becomes negligible downstream of cavity 5, consistent with the decay of SPL and the transition toward a linear regime in which vortex-shedding effects are weak [7]. Differences between the first and second orifice are negligible in this configuration.

When a turbulent grazing flow is introduced, the acoustic–vortical energy exchange becomes strongly phase dependent. The magnitude of Π^+_g increases significantly due to the enhanced effect of the grazing flow [10], and its spatial distribution becomes highly asymmetric. A quasi-steady recirculation in the upstream portion of the orifice shifts the vortex-shedding activity toward the downstream side, reflecting the modified flow topology. During the inflow phase, Π^+_g is predominantly positive, indicating acoustic energy transfer to vortical structures. The generated vortices are rapidly advected into the cavity by the acoustic-induced velocity. During the outflow phase, Π^+_g becomes predominantly negative: the jet-like outflow from the orifice interacts with the turbulent grazing flow in a manner analogous to a jet in crossflow, generating vorticity that feeds energy back into the acoustic field. The phase-resolved shedding rates are shown in figures 10(d,e). The inflow phase yields a positive contribution (net dissipation), whereas the outflow phase yields a negative contribution (net generation). Although both contributions are more than an order of magnitude larger than in the no-flow case, their imbalance results in a net negative cycle-averaged contribution for all cavities.

As the streamwise position increases, the magnitude of the acoustic energy conversion decreases due to the SPL decay but less markedly compared to the no-flow case. Consistently with the behaviour observed for viscous dissipation, the shedding contribution is higher for the second orifice than for the first one (subfigure e), due to the locally increased acoustic-induced velocity associated with the weakened shear layer.

E. Time-averaged volumetric dissipation density as a function of the streamwise coordinate

Figure 11 summarises the streamwise evolution of the time-averaged volumetric dissipation density, e^+. The values are scaled to represent the full three-dimensional orifice, following the approach of Scarano et al. [10]. Subfigure (a) shows the case without grazing flow, while subfigure (b) corresponds to the case with grazing flow. The contributions of the two orifices within each cavity are shown separately, while circle markers denote the cumulative contribution of both orifices. Shaded markers represent the vortex-shedding contribution, whereas unshaded regions correspond to viscous dissipation.

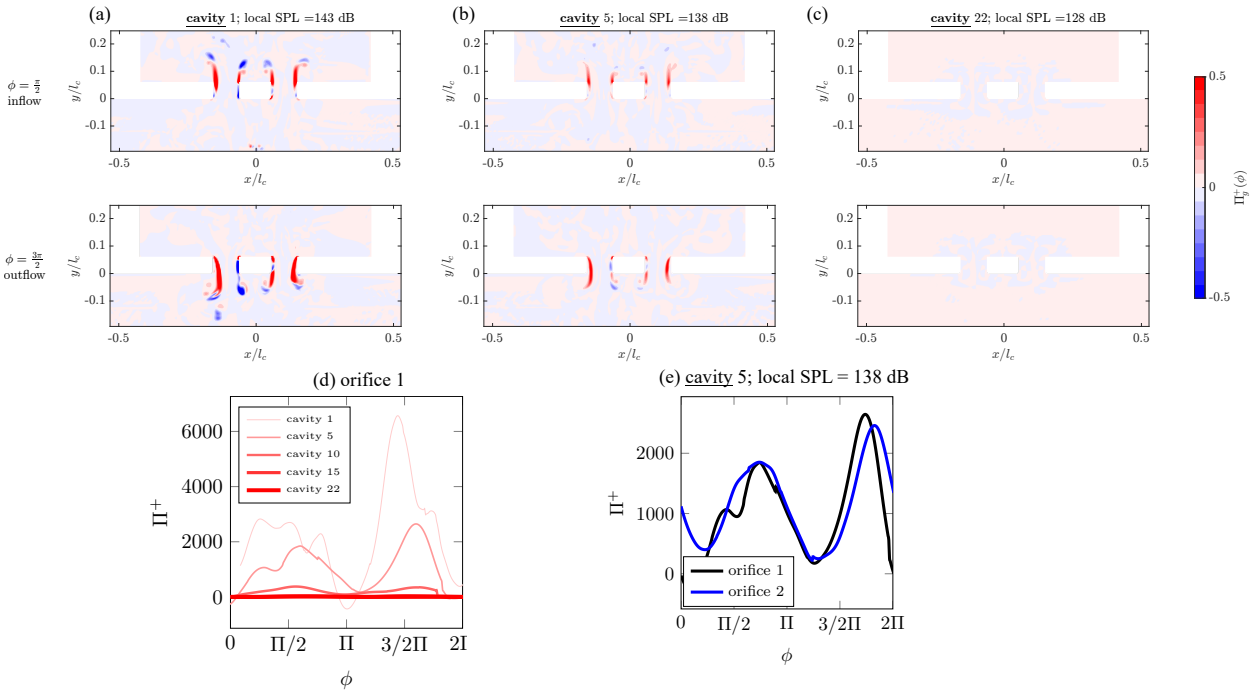

Fig. 9 Contour of the power density transferred between acoustic and vortical field, Π_g^+, in inflow and outflow phases at $M = 0$, forcing frequency equal to 1400 Hz, incident SPL = 145 dB (a) cavity 1, (b) cavity 10, (c) cavity 22; rate of the acoustic energy dissipation by vortex shedding Π^+ as a function of the phase, ϕ, (d) first orifice, effect of changing the cavity (e) cavity 10, comparison between orifice 1 and 2.

In the absence of grazing flow, both viscous and vortex-shedding contributions decrease monotonically along the liner, reflecting the progressive reduction of SPL in the streamwise direction. This reduction weakens the acoustic-induced velocity within the orifices and leads to lower dissipation rates. Vortex shedding is dominant in the first three cavities, where the SPL exceeds approximately 140 dB, indicating a strongly nonlinear regime. The viscous contribution dominates on the second half of the liner, in agreement with low-SPL or weakly nonlinear regimes [7]. The intersection of the cumulative viscous and shedding contributions marks the transition toward a regime where viscous dissipation prevails. This threshold is consistent with the single-cavity results reported by Scarano et al. [10].

When the turbulent grazing flow is introduced, the vortex-shedding contribution becomes negative for all cavities, indicating a net generation of acoustic energy. Its magnitude is largest on the first cavities and decreases downstream following the SPL decay. In contrast, the viscous contribution is enhanced over the entire liner compared to the no-flow case, due to the increased flow impingement on the downstream lip of the orifice. It decreases in the streamwise direction with a trend similar to that of the acoustic-induced velocity, although with a different slope compared to the no-flow case, suggesting that flow-induced effects partially compensate for the SPL decay. The second orifice contributes more significantly to both viscous dissipation and vortex-shedding generation, consistently with the locally increased v_{ac}^+.

The cumulative time-averaged volumetric dissipation density, obtained by combining viscous and vortex-shedding contributions, is reported in figure 12. In the absence of grazing flow, the acoustic dissipation is concentrated in the upstream portion of the liner, where nonlinear effects and vortex shedding are dominant, and decreases downstream with the SPL decay. This indicates that most of the acoustic energy is dissipated within the first ten cavities.

In contrast, when grazing flow is present, the net dissipation remains approximately constant along the liner. This behaviour results from a balance between enhanced viscous dissipation and negative vortex-shedding contributions. The increase in viscous dissipation, driven by higher local acoustic-induced velocities and flow impingement, is offset by the acoustic energy generation occurring during the outflow phase due to the interaction with the grazing flow. These findings highlight that the spatial distribution of dissipation mechanisms is fundamentally altered by the presence of grazing flow.

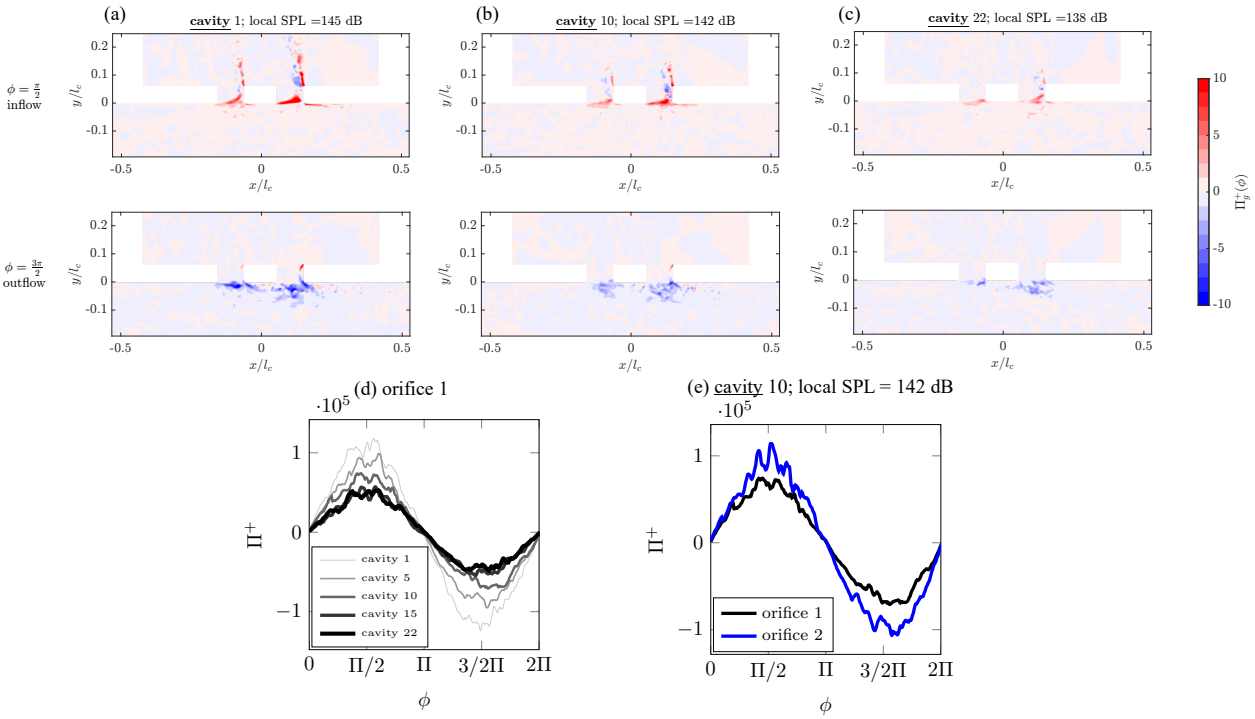

Fig. 10 Contour of the power density transferred between acoustic and vortical field, Π_g^+, in inflow and outflow phases at $M = 0.3$, forcing frequency equal to 1400 Hz, incident SPL = 145 dB (a) cavity 1, (b) cavity 10, (c) cavity 22; rate of the acoustic energy dissipation by vortex shedding Π^+ as a function of the phase, ϕ, (d) first orifice, effect of changing the cavity (e) cavity 10, comparison between orifice 1 and 2.

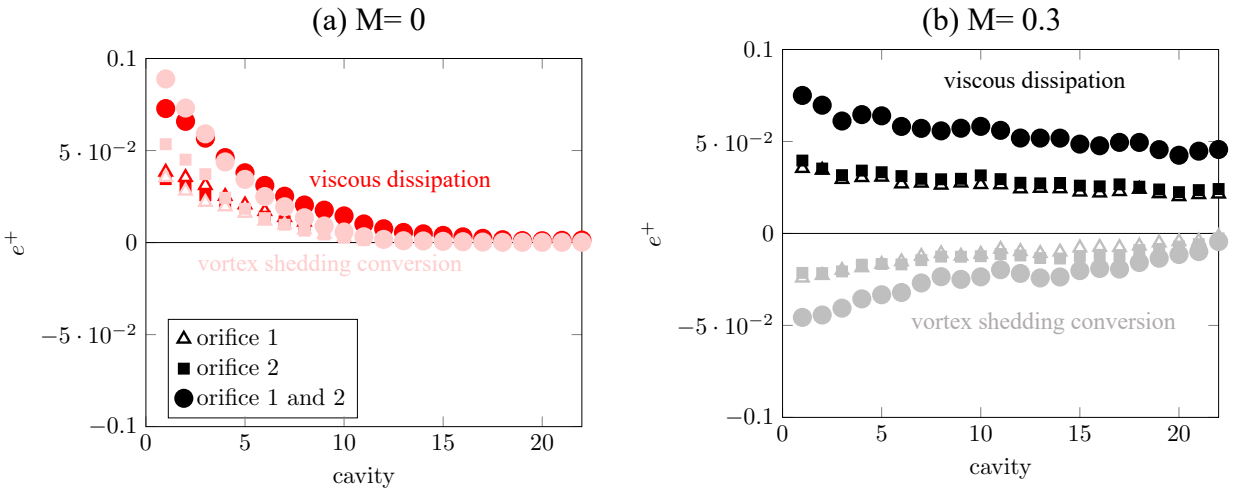

Fig. 11 Time averaged volumetric dissipation density as function of the streamwise coordinate, shaded color vortesh shedding dissipation, normal color viscous dissipation, (a) no-flow case, (b) $M = 0.3$ case.

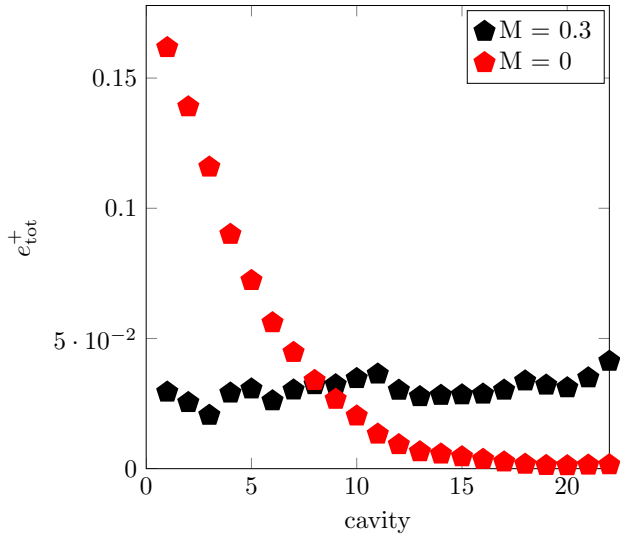

Fig. 12 Time averaged total volumetric dissipation density as function of the streamwise coordinate, comparison between no-flow case and $M = 0.3$ case.

V. Concluding remarks

This work analyzes the dissipation mechanisms over a 22-cavity acoustic liner with chamfered orifices using a high-fidelity dataset obtained from LBM/VLES simulations. The analysis is performed along the full liner, allowing the effect of the streamwise development of the grazing flow and the associated SPL decay to be taken into account.

The results highlight the strong influence of grazing flow on the dissipation mechanisms. In the absence of flow, viscous and vortex-shedding contributions are symmetric between inflow and outflow phases, with vortex shedding dominating in the upstream cavities at high SPL and viscous dissipation prevailing downstream as the SPL decreases.

When grazing flow is introduced, the flow topology inside the orifice is significantly modified. The formation of a quasi-steady vortex in the upstream portion of the orifice alters the distribution of the acoustic-induced velocity, leading to a concentration of viscous dissipation on the downstream lip during the inflow phase. At the same time, vortex shedding becomes strongly phase dependent: it contributes to dissipation during inflow and to acoustic energy generation during outflow. As a result, the net contribution of vortex shedding becomes negative over the entire liner.

The combined effect of these mechanisms leads to a substantial modification of the spatial distribution of dissipation. While in the absence of grazing flow the dissipation is concentrated in the upstream portion of the liner, in the presence of flow it remains approximately constant along the liner due to a balance between enhanced viscous dissipation and vortex-shedding generation. This implies that, with current liner designs, a sufficiently long liner is required to achieve effective noise absorption in the presence of grazing flow.

These findings explain the degradation of liner performance in the presence of grazing flow. The results indicate that current liner designs are not optimized to operate under grazing flow conditions, and that improvements should explicitly account for flow-induced effects, including the modification of the shear layer and the phase-dependent behaviour of vortex shedding. In particular, the optimization of orifice geometry and their spatial distribution appears essential to enhance overall acoustic dissipation.

VI. Acknowledgments

The work of A. Paduano, F. Scarano and F. Avallone is co-funded by the European Union (ERC, LINING, 101075903). Views and opinions expressed are however those of the author(s) only and do not necessarily reflect those of the European Union or the European Research Council. Neither the European Union nor the granting authority can be held responsible for them.

References

[1] Motsinger, R., and Kraft, R., "Design and performance of duct acoustic treatment," *Aeroacoustics of Flight Vehicles: Theory and Practice. Volume 2: Noise Control*, edited by H. Hubbard, NASA, 1991, Chap. 14, pp. 165–206. URL https://ntrs.nasa.gov/search.jsp?R=19920005565.

[2] Winkler, J., Mendoza, J., Reimann, C., Homma, K., and Alonso, J., "High fidelity modeling tools for engine liner design and screening of advanced concepts:," *International Journal of Aeroacoustics*, Vol. 0, No. 0, 2021, pp. 1–31. https://doi.org/10.1177/1475472X211023884, URL https://journals.sagepub.com/doi/full/10.1177/1475472X211023884.

[3] Mallat, S. G., "A Theory for Multiresolution Signal Decomposition: The Wavelet Representation," Tech. Rep. 7, 1989. https://doi.org/http://repository.upenn.edu/cisreports/668.

[4] Hughes, C., "The Promise and Challenges of Ultra High Bypass Ratio Engine Technology and Integration," *AIAA Aero Sciences Meeting*, 2011, pp. 0–11. URL www.nasa.govhttp://hdl.handle.net/2060/20110011737.

[5] Casalino, D., Hazir, A., and Mann, A., "Turbofan broadband noise prediction using the lattice boltzmann method," *AIAA Journal*, Vol. 56, No. 2, 2018. https://doi.org/10.2514/1.J055674.

[6] Motsinger, R. E., and Kraft, R. E., "4 Design and Performance of Duct Acoustic Treatment," Tech. rep., 1991.

[7] Tam, C. K. W., and Kurbatskii, K. A., "Microfluid Dynamics and Acoustics of Resonant Liners," *AIAA Journal*, Vol. 38, No. 8, 2000, pp. 1331–1339. https://doi.org/10.2514/2.1132, URL https://arc.aiaa.org/doi/10.2514/2.1132.

[8] Howe, M., "The dissipation of sound at an edge," *Journal of Sound and Vibration*, Vol. 70, No. 3, 1980, pp. 407–411. https://doi.org/10.1016/0022-460X(80)90308-9, URL https://linkinghub.elsevier.com/retrieve/pii/0022460X80903089.

[9] Zhang, Q., and Bodony, D. J., "Numerical investigation and modelling of acoustically excited flow through a circular orifice backed by a hexagonal cavity," *Journal of Fluid Mechanics*, Vol. 693, 2012, p. 367–401. https://doi.org/10.1017/jfm.2011.537.

[10] Scarano, F., Paduano, A., and Avallone, F., "Noise dissipation mechanisms of an acoustic liner under grazing flow," , 2025. URL https://arxiv.org/abs/2512.09587.

[11] Gaeta, R. J., and Ahuja, K. K., "Effect of orifice shape on acoustic impedance," *International Journal of Aeroacoustics*, Vol. 15, No. 4-5, 2016. https://doi.org/10.1177/1475472X16642133.

[12] Zhao, D., Ji, C., and Wang, B., "Geometric shapes effect of in-duct perforated orifices on aeroacoustics damping performances at low Helmholtz and Strouhal number," *The Journal of the Acoustical Society of America*, Vol. 145, No. 4, 2019. https://doi.org/10.1121/1.5096642.

[13] Cummings, A., "Acoustic nonlinearities and power losses at orifices," *AIAA Journal*, Vol. 22, No. 6, 1984. https://doi.org/10.2514/3.8680.

[14] Zheng, M., Chen, C., and Li, X., "The influence of the grazing flow and sound incidence direction on the acoustic characteristics of double Helmholtz resonators," *Applied Acoustics*, Vol. 202, 2023. https://doi.org/10.1016/j.apacoust.2022.109160.

[15] Paduano, A., Scarano, F., Cordioli, J., Casalino, D., and Avallone, F., "On the impact of the turbulent grazing flow development on the acoustic response of an acoustic liner," *arXiv preprint arXiv:2507.22714*, 2025.

[16] Paduano, A., Avallone, F., and Scarano, F., "On the role of orifice design in acoustic liner attenuation under turbulent grazing flow," *32nd AIAA / CEAS Aeroacoustics Conference*, American Institute of Aeronautics and Astronautics Inc, AIAA, 2026.

[17] Tam, C., Pastouchenko, N., Jones, M., and Watson, W., "Experimental validation of numerical simulations for an acoustic liner in grazing flow: Self-noise and added drag," *Journal of Sound and Vibration*, Vol. 333, No. 13, 2014, pp. 2831–2854. https://doi.org/10.1016/J.JSV.2014.02.019, URL https://www.sciencedirect.com/science/article/pii/S0022460X1400131X.

[18] Avallone, F., Manjunath, P., Ragni, D., and Casalino, D., "Lattice-boltzmann very large eddy simulation of a multi-orifice acoustic liner with turbulent grazing flow," *25th AIAA/CEAS Aeroacoustics Conference, 2019*, 2019. https://doi.org/10.2514/6.2019-2542.

[19] Scarano, F., Lyu, B., Paduano, A., and Avallone, F., "Filtering acoustic from hydrodynamic velocity using modal decomposition methods on an acoustic liner under grazing turbulent flow," , 2025. Submitted to Journal of Sound and Vibration.

[20] Howe, M. S., "Contributions to the theory of aerodynamic sound, with application to excess jet noise and the theory of the flute," *Journal of Fluid Mechanics*, Vol. 71, No. 4, 1975, pp. 625–673. https://doi.org/10.1017/S0022112075002777, URL https://www.cambridge.org/core/product/identifier/S0022112075002777/type/journal_article.

[21] Howe, M. S., "On the Absorption of Sound by Turbulence and Other Hydrodynamic Flows," *IMA Journal of Applied Mathematics*, Vol. 32, No. 1-3, 1984, pp. 187–209. https://doi.org/10.1093/imamat/32.1-3.187, URL https://academic.oup.com/imamat/article-lookup/doi/10.1093/imamat/32.1-3.187.

[22] Schmidt, O. T., and Colonius, T., "Guide to Spectral Proper Orthogonal Decomposition," *AIAA Journal*, Vol. 58, No. 3, 2020, pp. 1023–1033. https://doi.org/10.2514/1.J058809, URL https://arc.aiaa.org/doi/10.2514/1.J058809.

[23] Lyu, B., "Canonical correlation decomposition of numerical and experimental data for observable diagnosis," *30th AIAA/CEAS Aeroacoustics Conference*, 2024, pp. AIAA 2024–3206.

[24] Zhang, Q., and Bodony, D., "Numerical investigation and modelling of acoustically excited flow through a circular orifice backed by a hexagonal cavity," *Journal of Fluid Mechanics*, Vol. 693, 2012, pp. 367–401. https://doi.org/10.1017/jfm.2011.537, URL http://www.journals.cambridge.org/abstract_S0022112011005374.

[25] Léon, O., Méry, F., Piot, E., and Conte, C., "Near-wall aerodynamic response of an acoustic liner to harmonic excitation with grazing flow," *Experiments in Fluids*, Vol. 60, No. 9, 2019, p. 144. https://doi.org/10.1007/s00348-019-2791-5, URL http://link.springer.com/10.1007/s00348-019-2791-5.

[26] Roncen, R., "Revisiting nonlinear impedance in acoustic liners," *Journal of Sound and Vibration*, Vol. 608, 2025, p. 119058. https://doi.org/https://doi.org/10.1016/j.jsv.2025.119058, URL https://www.sciencedirect.com/science/article/pii/S0022460X25001324.

[27] Avallone, F., Khedr, A., Paduano, A., Scarano, F., Meirelles, L., and Cordioli, J., "On the relevance of facesheet orifice geometry to acoustic liner impedance," *npj Acoustics*, Vol. 2, 2026, p. 6. https://doi.org/10.1038/s44384-026-00044-x.

[28] Zhang, Q., and Bodony, D. J., "Numerical investigation of a honeycomb liner grazed by laminar and turbulent boundary layers," *Journal of Fluid Mechanics*, Vol. 792, 2016, pp. 936–980. https://doi.org/10.1017/jfm.2016.79, URL https://www.cambridge.org/core/product/identifier/S0022112016000793/type/journal_article.